JES
JOURNAL OF ENVIRONMENTAL SCIENCES
ISSN 1001-0742
CN 11-2629/X
December 1, 2014 Volume 26 Number 12
www.jesc.ac.cn

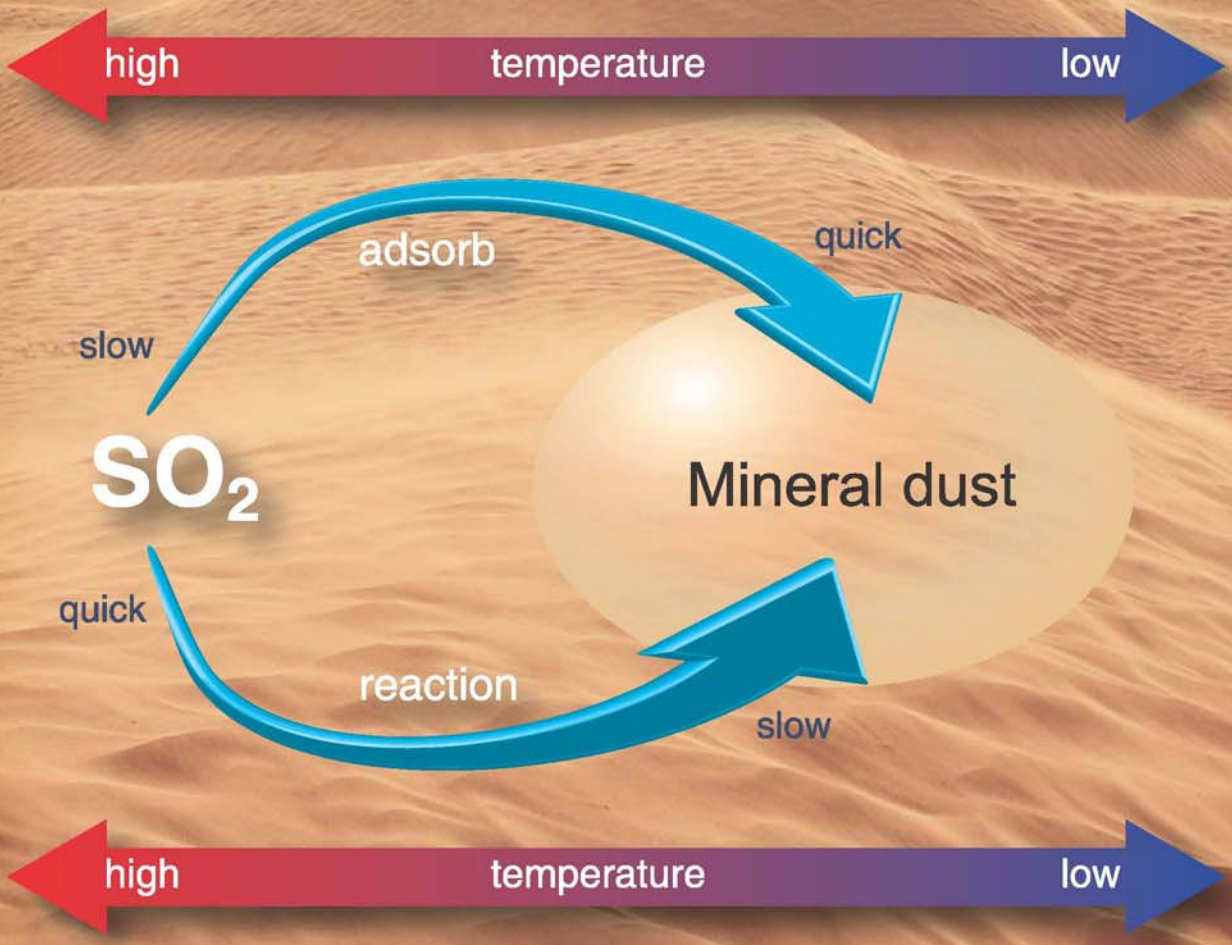

ELSEVIER
Science Press
Sponsored by
Research Center for Eco-Environmental Sciences
Chinese Academy of Sciences

Journal of Environmental Sciences Volume 26 Number 12 2014

www.jesc.ac.cn

CONTENTS

Available online at www.sciencedirect.com

ScienceDirect

www.journals.elsevier.com/journal-of-environmental-sciences

Combination of heterogeneous Fenton-like reaction and photocatalysis using Co–TiO_2 nanocatalyst for activation of $KHSO_5$ with visible light irradiation at ambient conditions

Qingkong Chen[1,2,3], *Fangying Ji*[2,3,*], *Qian Guo*[4], *Jianping Fan*[2,3], *Xuan Xu*[2,3]

1. *School of River and Ocean Engineering, Chongqing Jiaotong University, Chongqing 400074, China. E-mail: chenqingkong@126.com*
2. *Key Laboratory of Three Gorges Reservoir Region's Eco-Environment, Ministry of Education, Chongqing University, Chongqing 400045, China*
3. *National Centre for International Research of Low-carbon and Green Buildings, Chongqing University, Chongqing 400045, China*
4. *T.Y. Lin International Engineering Consulting (China) Co., Ltd, Chongqing 401121, China*

ARTICLE INFO

Article history:
Received 16 January 2014
Revised 5 March 2014
Accepted 11 April 2014
Available online 31 October 2014

Keywords:
Fenton-like
Photocatalysis
Cobalt
Sulfate radical
Visible light

ABSTRACT

A novel coupled system using Co–TiO_2 was successfully designed which combined two different heterogeneous advanced oxidation processes, sulfate radical based Fenton-like reaction (SR-Fenton) and visible light photocatalysis (Vis-Photo), for degradation of organic contaminants. The synergistic effect of SR-Fenton and Vis-Photo was observed through comparative tests of 50 mg/L Rhodamine B (RhB) degradation and TOC removal. The Rhodamine B degradation rate and TOC removal were 100% and 68.1% using the SR-Fenton/Vis-Photo combined process under ambient conditions, respectively. Moreover, based on XRD, XPS and UV-DRS characterization, it can be deduced that tricobalt tetroxide located on the surface of the catalyst is the SR-Fenton active site, and cobalt ion implanted in the TiO_2 lattice is the reason for the visible light photocatalytic activity of Co–TiO_2. Finally, the effects of the calcination temperature and cobalt concentration on the synergistic performance were also investigated and a possible mechanism for the synergistic system was proposed. This coupled system exhibited excellent catalytic stability and reusability, and almost no dissolution of Co^{2+} was found.

Introduction

Advanced oxidation processes (AOPs), which can rapidly destroy a wide range of recalcitrant organic compounds in wastewater, have emerged as an attractive alternative to conventional waste water treatment (*e.g.*, coagulation/flocculation and active sludge technologies). Such effective removal of aquatic hazardous substances is ascribed to generation of highly reactive transient species (*e.g.*, $^{\cdot}OH$) by various means (*e.g.*, UV/O_3, UV/H_2O_2, Fenton and photocatalysis). The hydroxyl radical ($^{\cdot}OH$) exhibits approximately nonselective reactivity toward diverse organic molecules and can degrade organic pollutants into CO_2 and H_2O theoretically (Buxton et al., 1988; Shen et al., 2007, 2009). However, different AOPs usually have different treatment requirements, which means high operation cost and confines the application of individual technologies. Instead of using a single AOT, the combination of two or more AOPs to produce a synergistic effect has been found to be effective in enhancing the performance of individual processes as well as being cost-effective (Rey et al., 2011). For instance, when homogeneous Fenton is combined with TiO_2-photocatalysis, the pollutant

* *Corresponding author*. E-mail: jfy@cqu.edu.cn (Fangying Ji).

http://dx.doi.org/10.1016/j.jes.2014.03.003
1001-0742/

removal efficiency is enhanced (Quici et al., 2005; Selvam et al., 2007; Lee et al., 2003). However, simple combination of iron-Fenton with TiO_2-photocatalysis still requires acidic pH and UV irradiation; moreover, the resulting iron-sludge also means high disposal cost.

In recent years, a new Co(II)/$KHSO_5$ homogenous/heterogeneous Fenton-like catalysis has been developed (Anipsitakis and Dionysiou, 2004), which exhibited a much higher degradation efficiency than traditional iron-Fenton in a wider pH range, from 2 to 9 (Anipsitakis et al., 2006). Now, the process is referred to as the sulfate radical based Fenton-like reaction (SR-Fenton), since the main active species of this system is sulfate radical ($SO_4^{\cdot-}$). The $SO_4^{\cdot-}$ radical has been demonstrated to have a higher standard reduction potential (2.5–3.1 V) than $^{\cdot}OH$ (1.8–2.7 V) at neutral pH (Chan and Chu, 2009), hence the SR-Fenton may overcome the pH limitation of conventional Fenton. On the other hand, among a number of TiO_2 modification studies, we also find the utilization of cobalt to enhance its photocatalytic activity or extend the photoresponse of TiO_2 into the visible light region (Vis-Photo). For example, Le et al. (2012) reported water splitting using a Co-doped TiO_2 composite under visible light. Thus, the transition metal Co is a common factor in these two AOTs, and we could hypothesize that the coupling of Co and TiO_2 could possibly form a kind of catalyst that possesses both SR-Fenton and Vis-Photo catalytic activities. Furthermore, a heterogeneous combined SR-Fenton/Vis-Photo system based on this catalyst could be built to eliminate organic pollutants in water.

In this study we synthesized a Co–TiO_2 nanocatalyst using a sol–gel method, and the dye Rhodamine B (RhB) was used as a model pollutant. The synergistic effect of SR-Fenton and Vis-Photo was observed when Co–TiO_2, $KHSO_5$ and visible irradiation were present simultaneously. This effect resulted in dramatic kinetic enhancement in RhB oxidation and TOC removal at neutral pH. Moreover, the cobalt concentration and calcination temperatures influenced the synergistic performance greatly.

1. Experimental

1.1. Chemicals and materials

Cobalt nitrate ($Co(NO_3)_2{\cdot}6H_2O$) was purchased from Chengdu Kelong Chemical Reagent Co., Ltd., Chengdu, China. Tetra-n-butyl titanate ($C_{16}H_{36}O_4Ti$) was obtained from Shanghai Qiangshun Co., Ltd., Shanghai, China. Rhodamine B (RhB) was obtained from Tianjin Guangfu Fine Chemical Research Institute, Tianjin, China. $KHSO_4$ was purchased from Aladdin Chemical Reagent Co., Ltd., Shanghai, China. All chemicals used in this study were analytical grade reagents and were used as received without further purification. Deionized water was used in the present work.

1.2. Preparation of Co–TiO_2 nanoparticles

Co–TiO_2 catalysts were prepared by a sol–gel method. A stoichiometric amount of tetrabutyl titanate and citric acid was dissolved in ethanol to form solution A; $Co(NO_3)_2$ (dissolved in deionized water first) was also dissolved in ethanol to form solution B. Then solution B was added to solution A drop by drop with continuous stirring. After gelation, the solids were aged for 48 hr, and the gels were dried in an oven at 110°C to remove water. Finally, the catalysts were calcined in a furnace at 400, 500 or 600°C for 6 hr with a ramp rate of 10°C/min. The molar percentages of Co were 0.5%, 1.0% and 1.5%, respectively. The resulting Co–TiO_2 catalysts were labeled as XCo–$YTiO_2$, where X stands for the molar percentage of Co and Y stands for the calcination temperature. The preparation procedure of pure TiO_2 catalyst was the same as that for Co–TiO_2.

1.3. Degradation experiment

The catalytic activity tests of three systems (Co–TiO_2/$KHSO_5$, Vis/Co–TiO_2 and Vis/Co–TiO_2/$KHSO_5$) were evaluated in terms of RhB degradation. RhB, a typical toxic dye, is relatively stable to visible light irradiation (Ma and Yao, 1999) and its absorption spectrum is not influenced by pH variation significantly in aqueous solutions (Sridharan and Park, 2013). Therefore, it is widely used to assess the catalytic activity of Fenton- or photo-catalysts (Wang and Zhang, 2011; Gao et al., 2013; Liu et al., 2012). All the experiments were performed in a glass cylindrical reactor containing 500 mL of RhB solution with pH adjusted to 7.0 using 0.5 mol phosphate buffer (Liu et al., 2012; Goulden and Anthony, 1978) and placed on a magnetic stirrer plate. The temperature of the reaction solution was kept at 25 ± 2°C by an external cooling water system in the Photo and SR-Fenton/Vis-Photo processes. (1) SR-Fenton (Co–TiO_2/$KHSO_5$): after the addition of 0.5 g of Co–TiO_2 catalyst (1.0 g/L), the solution was allowed to reach adsorption equilibrium between the catalyst and RhB (there was no appreciable RhB adsorption on the surface of the samples, Fig. S1). Then, $KHSO_5$ was added into the solution at [$KHSO_5$]: [RhB] molar ratio of 4:1. To measure the degradation rate of RhB during 2 hr of reaction, 2 mL samples were withdrawn at specified time intervals and quenched with 2 mL of methanol to prevent further reaction. (2) Vis-Photo (Vis/Co–TiO_2): the photocatalytic experiments were conducted under ambient atmospheric conditions. The artificial visible light source was a 1000 W Xe arc lamp (Yaming, Shanghai, China) illuminating the top of the reactor from 10 cm distance in a light-shielded box. All the UV light with wavelength shorter than 420 nm was removed by a cut-off filter (JB420, Shanghai, China). In order to ensure adsorption equilibrium, the solution was stirred for about 45 min in the dark first. (3) SR-Fenton/Vis-Photo (Vis/Co–TiO_2/$KHSO_5$): the experimental conditions and test methods were the same as (1), with the 1000 W Xe arc lamp with light filter ($\lambda \geq 420$ nm) as the light source.

1.4. Reaction quenching study

In order to classify the types of active radicals present in the reaction system and their role, quenching tests were carried out to determine the active radicals. Two different types of alcohols, *viz.*, ethanol and tertiary butanol, were used as quenching reagents with different concentrations. Ethanol is capable of quenching both sulfate and hydroxyl radicals as it has a high reactivity towards both radicals, whereas tertiary butanol mainly reacts with hydroxyl radical and much more slowly with sulfate radical (Shukla et al., 2010; Ji et al., 2011).

1.5. Stability and reusability of the catalyst

The stability and reusability of the catalysts were evaluated in three aspects: (1) structural stability of the catalyst; (2) cobalt leaching from the catalyst; (3) catalytic activity over multiple runs. So, the spent catalyst was recovered from the reaction

mixture by filtration and washed thoroughly with deionized water and dried at 80°C for reuse. In order to evaluate the structural stability of the catalyst, the crystallographic structure of the fresh and spent catalyst (2 hr × 5 runs) was investigated by XRD. Furthermore, the surface composition of the catalyst was tested by XPS. Five recycling runs of the Co–TiO_2 catalyst (1.0Co–500TiO_2) were conducted, and the catalyst was recycled under the same reaction conditions to evaluate the reusability of the Co–TiO_2 catalyst. After every run, the suspensions were centrifugated and the catalyst was collected, washed thoroughly, and dried in an oven at 80°C before the next round.

1.6. Characterization and analytical methods

The cobalt mass fractions of the fresh samples were measured by an X-ray fluorescence spectrometer (PPM-100%, Baird, USA). The crystallographic structure and phase composition of Co–TiO_2 catalysts was investigated with an X-ray diffractometer (XRD-6000, Shimadzu, Japan) with Cu Kα (λ = 1.5406 Å) radiation. The crystallite size was calculated by the Scherrer equation (Eq. (1)) (Anderson and Bard, 1995) and the phase content of samples was measured by the reference intensity ratio (RIR) method (Eq. (2)) (Hiller, 2000).

$$\tau = \frac{K\lambda}{\beta \cos\theta} \tag{1}$$

where,

τ is size of the ordered (crystalline) domains;
K is a dimensionless shape factor;
λ is X-ray wavelength;
β is the line broadening at half the maximum intensity (FWHM);
θ is Bragg angle.

$$RIR_{i,s} = \left[\frac{X_s}{Xi}\right]\left[\frac{I_{(hld)i}}{I_{(hld)'s}}\right]\left[\frac{I^{rel}{}_{(hld)'s}}{I^{rel}{}_{(hld)i}}\right] \tag{2}$$

where,

X is weight fraction,
I is intensity,
I^{rel} is relative intensity and the subscripts i and s indicate phase i and the standard phases, respectively.

An ASAP-2010 (Micromeritics, USA) surface area and porosimetry analyzer was used to determine the Brunauer–Emmett–Teller (BET) surface area of the catalysts. The morphology of the catalysts was measured by an environmental field emission scanning electron microscope (FEI, USA) equipped with a EDS system. In order to determine the chemical states on the catalyst surface, an X-ray photoelectron spectroscope (Amicus, Shimadzu, Japan) with Mg Kα X-ray source was used. UV–vis diffuse reflectance spectra and three-dimensional excitation–emission matrix fluorescence spectra were obtained under atmospheric conditions using a UV–vis spectrophotometer (UV3010, Hitachi, Japan) equipped with an integrating sphere attachment and a fluorescence spectrophotometer (F-7000, Hitachi, Japan). The band gap energy (E_g) of 1.0Co–500TiO_2 was calculated using the Kubelka–Munk function (Eq. (3)) (Liu et al., 2008; Ganesh et al., 2012; Cao et al., 2013):

$$(\alpha h\nu)^{1/2} = A(h\nu - E_g) \tag{3}$$

where, E_g is the optical band gap of the catalyst and A is a constant.

The degradation samples were centrifugated at 4500 r/min for 15 min and the RhB concentration was analyzed using a UV–vis spectrophotometer (UV3010, Hitachi, Japan) at the wavelength of 552 nm. The concentration of $KHSO_5$ was analyzed by a titration method (Liang et al., 2007). Total organic content (TOC) present in the samples was determined using a Multi N/C 2100 analyzer (Analytik Jena, Germany). Moreover, the cobalt leaching with time was monitored by an atomic absorption spectrometer (Hitachi 180-80, Japan). All chemicals used in this study were analytical grade reagents and were used as received without further purification. Deionized water was used in the present work. All measurements were repeated three times and the results were reproducible within the experimental error (±3%).

2. Results and discussion

2.1. Co–TiO_2 catalyst characterization

Fig. 1 represents XRD spectra of pure TiO_2 and Co–TiO_2 samples, which were prepared with different cobalt concentrations (C_{cobalt}) and calcination temperatures (T_{cal}). In TiO_2 the relative abundance of rutile and anatase phases strongly depends on the thermal treatment. The XRD pattern (Fig. 1a) shows a single phase for calcination at 400°C (anatase) and 600°C (rutile) respectively. However, the anatase and rutile phases coexisted in pure TiO_2 and Co–TiO_2 at 500°C. Thus, 500°C can be considered as the phase transition temperature in our tests. In addition, with the increase of T_{cal}, the percentage of rutile phase increased gradually (Table 1), the diffraction peaks became sharper, the crystallite sizes (Table 1) became larger and the crystalline quality clearly improved. However, the cobalt seemed to inhibit the anatase to rutile phase conversion and elevated the content of the anatase phase (Fig. 1b, Table 1). When C_{cobalt} was 1.0%, the anatase percentage reached a maximum (70.6%). This shift in the anatase–rutile phase transition on addition of cobalt provides evidence for structural cobalt doping. No diffraction peaks of cobalt oxide phases were detected. This indicates either that the concentration of cobalt oxide formed in the samples was too low to be measured or that the cobalt ions were doped into the TiO_2 lattice. Since the Co^{2+} ionic radius (0.65 Å) is smaller than that of Ti^{4+} (0.69 Å) (Liu et al., 2008), the decrease in the lattice constants with cobalt concentration increasing from 0% to 1.5% (Table 2) also indicates that part of the cobalt ions were successfully incorporated into the host TiO_2 matrix.

The morphology of the Co–TiO_2 samples was investigated by FESEM. The particles were ball-like (Fig. 2a) with average diameter of about 20 nm. This is very similar to the crystal size data calculated by the Scherrer equation (Table 1). EDS

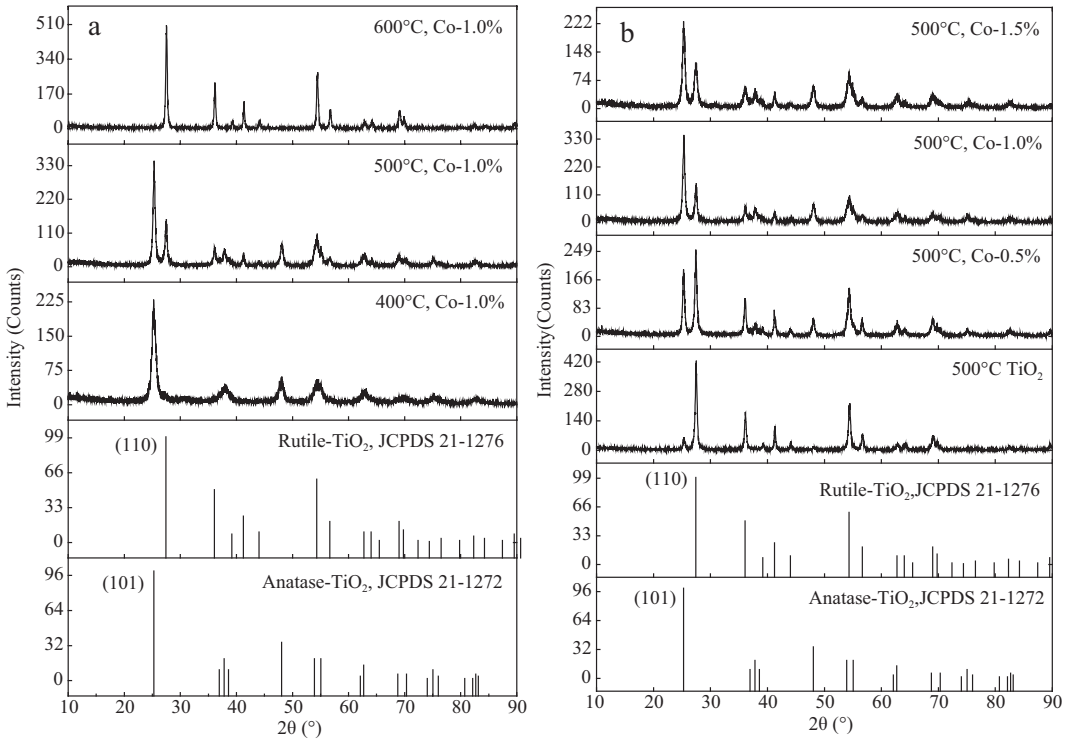

Fig. 1 – XRD patterns of Co–TiO_2 with different calcination temperatures (a) and Co–TiO_2 with different cobalt contents (b).

(Fig. 2b) clearly shows the main elemental composition of Co, Ti, C, and O. The cobalt mass fractions of in fresh catalysts were measured by X-ray fluorescence spectroscopy (XRF) and are shown in Table 3. The specific surface area (S_{BET}) values are listed in Table 1. High temperature calcination severely reduced S_{BET}, but cobalt doping appeared to enlarge it with increasing concentration. As shown in Fig. S1, all samples reached RhB adsorption equilibrium within the first 40 min, and the maximum adsorption was only 8.0%. Thus, there was no appreciable RhB adsorption on the surface of Co–TiO_2. All RhB degradation efficiency data shown in this paper have been corrected for the by the catalysts.

2.2. Catalytic activity of Co–TiO_2

Comparative experiments of RhB degradation were carried out to test the catalytic activity of the prepared Co–TiO_2 catalysts. The degradation of 50 mg/L of RhB as a function of reaction time is shown in Fig. 3. As shown in Fig. 3a, adsorption in the dark and visible light direct photolysis did not cause a significant loss of RhB. It was also seen that, approximately 33.5% of RhB was degraded in 120 min for the case of Dark/$KHSO_5$ or Vis/$KHSO_5$. Thus, the visible light cannot enhance the oxidation of RhB with $KHSO_5$. Fig. 3b illustrates the degradation tests for $KHSO_5$ only, SR-Fenton, Vis-Photo and SR-Fenton/Vis-Photo processes. The degradation rate reached 77.3% using the SR-Fenton and 45.7% in the Vis-Photo at neutral pH, which were both higher than the $KHSO_5$ alone; moreover, the RhB was degraded completely (100%) in the combined system within the first 80 min. It was revealed that the combined effect of Fenton and photocatalysis enhanced the removal of RhB significantly. In order to observe this synergistic effect more clearly, the RhB initial concentration was increased to 100 mg/L. From Fig. 3c, we

Table 1 – Structural property of catalysts.

Sample	S_{BET} [a] (m^2/g)	Crystallinity (%)	Crystal size [b] (nm)		Phase content (%)	
			Anatase	Rutile	Anatase	Rutile
TiO_2, 500°C	10.5	67.4	20.5	21.9	10.4	89.6
1.0Co–400TiO_2	65.0	17.8	13.0	/	100	/
0.5Co–500TiO_2	22.1	75.4	20.4	20.3	35.1	64.9
1.0Co–500TiO_2	28.4	69.3	18.7	18.8	70.6	29.4
1.5Co–500TiO_2	33.8	66.2	16.5	15.2	66.3	33.7
1.0Co–600TiO_2	2.6	65.1	/	26.3	/	100

[a] S_{BET}: BET specific surface area.
[b] (101) for anatase TiO_2, (110) for rutile TiO_2.

Table 2 – Cell parameters of the samples.

Sample	Phase	Cell parameters		
		a	*b*	*c*
TiO_2, 500°C	Anatase	3.7951	3.7951	9.4438
	Rutile	4.5861	4.5861	2.9589
1.0Co–400TiO_2	Anatase	3.7904	3.7832	9.4325
	Rutile	/	/	/
0.5Co–500TiO_2	Anatase	3.7942	3.7942	9.4429
	Rutile	4.5852	4.5852	2.9580
1.0Co–500TiO_2	Anatase	3.7930	3.7930	9.4400
	Rutile	4.5832	4.5832	2.9577
1.5Co–500TiO_2	Anatase	2.7917	2.7917	9.3980
	Rutile	4.5798	4.5798	2.9543
1.0Co–600TiO_2	Anatase	/	/	/
	Rutile	4.5922	4.5922	2.9682

were surprised to find that the efficiency of the SR-Fenton/Vis-Photo system for RhB oxidation exceeded the sums of the efficiencies of the two individual systems, SR-Fenton plus Vis-Photo.

As the ultimate aim of advanced oxidation technology is to oxidize the organic pollutants to CO_2 and H_2O completely, TOC removal efficiency is the accepted standard for evaluation of a new AOT. In contrast with 44.1% removal by SR-Fenton and 18.6% by Photo, the combined process reached 68.1% TOC removal rate, when the initial RhB concentration was 50 mg/L (Fig. 4). Furthermore, when the initial concentration was doubled, the TOC removal rate followed the same trend as RhB degradation. So, we can say the synergistic effect not only enhanced the RhB degradation, but also promoted the TOC removal remarkably. Therefore, two conclusions can be reached: (1) The Co–TiO_2 catalyst was demonstrated to have both SR-Fenton and visible light photocatalytic activity at neutral pH; (2) The SR-Fenton/Vis-Photo combined process showed a synergistic effect in the combination of SR-Fenton reaction and visible light photocatalysis.

Why does Co–TiO_2 have SR-Fenton and visible light photocatalytic activity simultaneously? We investigated the chemical and optical properties of Co–TiO_2 catalysts using XPS and UV–vis DRS spectra. XPS measurements were used to investigate the oxidation states of cobalt on the surface of the Co–TiO_2 catalyst. As shown in Fig. 5a, there are two strong symmetric peaks centered at 458.1 and 463.8 eV, which are in agreement with the binding energies of Ti $2p_{3/2}$ and Ti $2p_{1/2}$, respectively (Liu et al., 2008; Huang et al., 2009; Ganesh et al., 2012; Ding et al., 2012). This confirms that Ti is present as Ti^{4+}. The broad and asymmetric O 1s peak can be fitted by two nearly Gaussian components, centered at 529.7 and 531.7 (Liu et al., 2008; Huang et al., 2009; Ganesh et al., 2012; Ding et al., 2012) (Fig. 5b). The first peak on the low BE side of the O 1s spectrum (529.7 eV) was assigned to the O^{2-} ions in the lattice oxygen species from TiO_2 and Co_3O_4, and a shoulder at the higher binding energy of 531.7 eV to surface hydroxyl groups (*i.e.*, Ti–OH and Co–OH) that are ubiquitous in air-exposed cobalt oxide materials (Yang et al., 2007). Fig. 5c shows the XPS spectrum of the Co 2p region. We can find two major peaks with binding energies at 780.2 and 796.2 eV in the Co 2p XPS spectra, corresponding to Co $2p_{3/2}$ and Co $2p_{1/2}$, respectively, which is characteristic of a Co_3O_4 phase (Ganesh et al., 2012; Ding et al., 2012; Yang et al., 2007; Lu et al., 2011; Shi et al., 2012). During preparation of the catalyst, the white color of TiO_2 was changed to a green color with addition of cobalt, which indicated the deposition of cobalt oxide on the surface of the TiO_2 particles (Long et al., 2006). The color of the Co–TiO_2 composite powders became darker and darker with increasing cobalt concentration and calcination temperature. Compared to the spectrum of pure TiO_2, new absorption bands appeared between 400–800 nm in the Co–TiO_2 samples, which means that the band gap absorption onset was extended into the visible light region, with an absorption fringe between 760–800 nm (Fig. 6a and b). This obvious red shift should be attributed to the substitution of Co^{2+} for Ti^{4+} in the crystal lattice. Thus, a portion of the Co^{2+} ions were incorporated into the TiO_2 lattice and an impurity energy level was formed. The absorption bands at 200–400 nm are due to the charge transfer from the valence band to the conduction band of TiO_2. As previously reported (Jayakumar et al., 2009; Kim et al., 1994), the absorption band in the visible light region 520–700 nm can be assigned to the $^2E(G)$, $^4T_1(P)$, $^2A_1(G) \rightarrow$ ground state $^4A_2(F)$ transitions for high-spin Co^{2+} ($3d^7$) in tetrahedral coordination. The absorptions at 420 and 700 nm for Co–TiO_2 can be assigned to the $^1A_{1g} \rightarrow {}^1T_{2g}$ and $^1A_{1g} \rightarrow {}^1T_{1g}$ transitions of Co^{3+} ions in octahedral symmetry

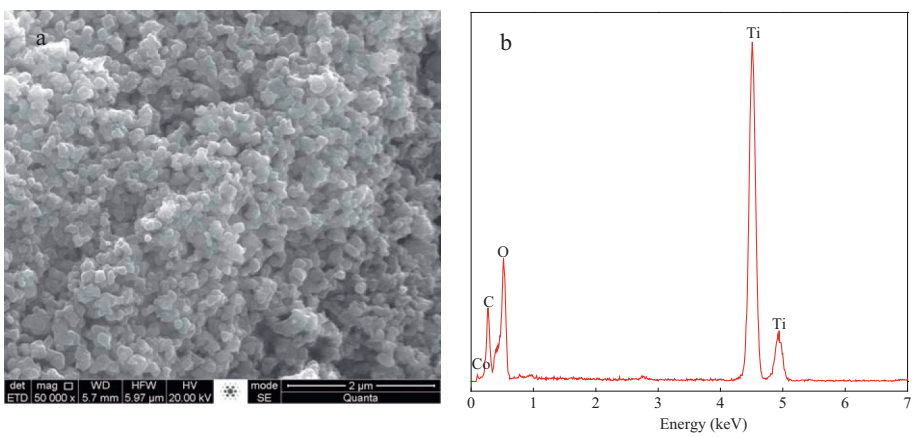

Fig. 2 – FESEM images (a) and EDS spectrum (b) of 1.0Co–500TiO_2.

Table 3 – Homogenous processes by leached Co^{2+} from the catalysts.

Sample	Mass fraction of cobalt [a] (%)	Concentration of leached Co^{2+} [b] (mg/L)	Leached cobalt percentage of total cobalt [c] (%)	Degradation efficiency of RhB (%)
1.0Co–400TiO_2	0.653	0.365	5.42	66.7
0.5Co–500TiO_2	0.344	0.051	1.48	8.2
1.0Co–500TiO_2	0.688	0.110	1.60	23.3
1.5Co–500TiO_2	1.022	0.231	2.25	41.5
1.0Co–600TiO_2	0.713	0.007	0.10	6.0

[a] Mass fraction of cobalt: tested by XRF, and calculated with 1.0 g catalysts.
[b] Concentration of leached Co^{2+}: tested by AAS.
[c] Leached Co^{2+} percentage of total cobalt: calculated with 1.0 g catalysts and by the equation percentage $= \frac{C_L}{C_T} \times 100\%$; C_L = leached cobalt content (mg), C_T = total cobalt content in the fresh catalysts (mg).

(Zayat and Levy, 2000). The band gap energy (E_g) of 1.0Co–500TiO_2 was calculated using the Kubelka–Munk function. The value was 1.56 eV for 1.0Co–500TiO_2 (Fig. 6b, insert). Based on the analysis above, it can be predicted that the Co–TiO_2 catalyst should possess visible photocatalytic activity, and this has been proved by experiment.

2.3. *Effect of cobalt concentration (C_{cobalt})*

The RhB degradation performance of Co–TiO_2 with different C_{cobalt} in Co–TiO_2/$KHSO_5$, Vis/Co–TiO_2 and Vis/Co–TiO_2/$KHSO_5$ processes is illustrated in Fig. 7. In general, the higher C_{cobalt} is, the faster and more complete the decay of RhB in the SR-Fenton (Co–TiO_2/$KHSO_5$) process. Higher C_{cobalt} will generate more active sites (Co_3O_4) for $KHSO_5$ decomposition, thus the degradation efficiency increases (Shi et al., 2012; Anipsitakis et al., 2005; Muhammad et al., 2012). However, 1.0% C_{cobalt} appears to be the most efficient in the Photo (Vis/Co–TiO_2) process. When Co–TiO_2 is excited by visible light, the cobalt ions incorporated into the TiO_2 lattice have two functions: one is to trap photo-excited electrons and holes (e_{cb}^-/h_{vb}^+); another is to induce impurity energy levels near the

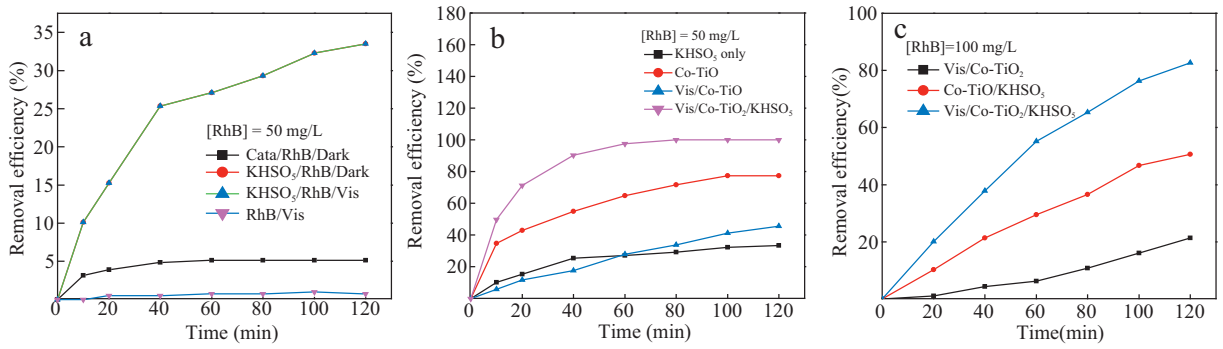

Fig. 3 – Degradation curves of RhB under different conditions. (a) and (b) 1.0Co–500TiO_2 used, [RhB] = 50 mg/L (0.1 mmol), [KHSO5] = 0.4 mmol, [Cata] = 1.0 g/L, pH = 7.0, 25°C, 2 hr; (c) 1.0Co–500TiO_2 used, [RhB] = 100 mg/L (0.2 mmol), [$KHSO_5$] = 0.4 mmol, [Cata] = 1.0 g/L, pH = 7.0, 25°C, 2 hr.

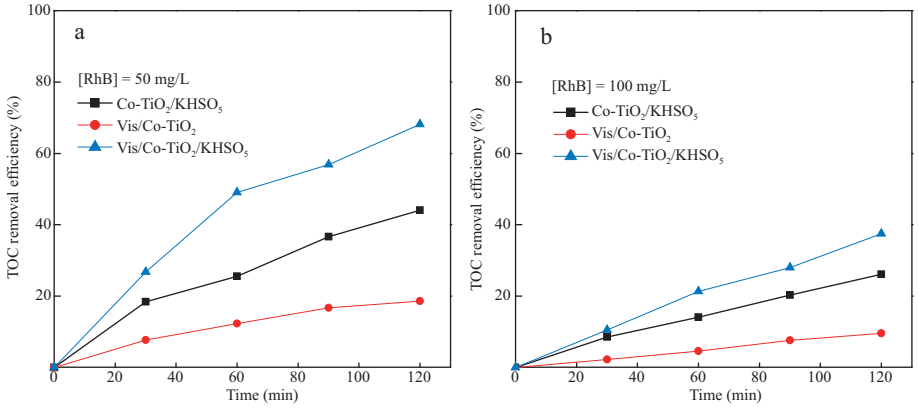

Fig. 4 – TOC removal under different processes. Conditions: 1.0Co–500TiO_2 used, [RhB] = 50 mg/L (0.1 mmol), [$KHSO_5$] = 0.4 mmol, [Cata] = 1.0 g/L, pH = 7.0, 25°C, 2 hr.

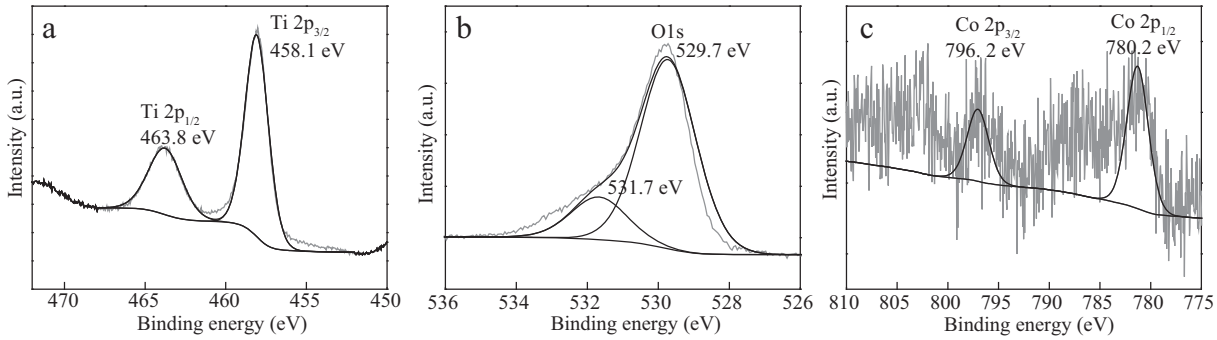

Fig. 5 – XPS survey spectra of 1.0Co–500TiO$_2$. (a) Ti 2p XPS spectra; (b) O 1s XPS spectra; (c) Co 2p XPS spectra.

conduction band as well as the valence band edge of TiO_2 (Ram et al., 2011). But only appropriate C_{cobalt} levels will promote electron–hole pair separation effectively. If the concentration is lower (*e.g.*, 0.5% in our tests), there are insufficient traps, otherwise, the cobalt ion will serve as an electron–hole recombination center. In order to characterize the separation/combination of photo-excited electrons and holes in Co–TiO_2, a three dimensional excitation–emission matrix fluorescence (EEM) was used to investigate the photoluminescence spectra (PL spectra) of the catalysts (Hu et al., 2009). The combination of photo-excited electron–hole pair will make the photocatalyst emit fluorescence (Xu, 2010), so the EEM spectrum of a system can be considered the result of electron–hole separation, electron phonon scattering and electron–hole combination. From Fig. S2, two strong peaks at Ex/Em 275/305 nm and Ex/Em 230/305 nm seen in all spectra are the characteristic spectra of TiO_2, and the fluorescence intensity reflects the behavior of electron–hole separation/combination (Xu, 2010). The weaker the fluorescence emitted, the easier it is for electrons and holes to separate. Compared to pure TiO_2 (Fig. S2a), the fluorescence intensity of 1.0Co–500TiO_2 diminished noticeably, but that of 1.5Co–500TiO_2 increased. Therefore, the quantum efficiency of 1.0Co–500TiO_2 was the highest. Apart from this, as pointed out by many investigators, the photocatalytic activity of anatase TiO_2 is better than rutile phase, thus the better photocatalytic activity of 1.0Co–500TiO_2 may be partly owing to the higher percentage of anatase phase (Table 1). The RhB degradation efficiency of the combined process also changed with C_{cobalt} (Fig. 7c), but the synergistic effect was not shown when using 0.5Co–TiO_2 and 1.5Co–500TiO_2. This result indicates that 1.0% is the optimal cobalt concentration.

2.4. *Effects of calcination temperature*

As shown in Fig. 8, SR-Fenton, Photo and SR-Fenton/Vis-Photo combined processes were affected by calcination temperature (T_{cal}). Many investigators have demonstrated that the activity of a heterogeneous SR-Fenton catalyst is positively related with its S_{BET} and leached ion concentration. Thus, the SR-Fenton activity of Co–TiO_2 shows the order: 1.0Co–400TiO_2 > 1.0–500TiO_2 > 1.0Co–600TiO_2. However, the photocatalytic activity of Co–TiO_2 catalysts did not follow the same trend. 1.0Co–400TiO_2 showed almost no photocatalytic activity (except for adsorption). This may ascribe to its lower crystallinity (Table 1), which would result in less effective separation of photo-excited electrons and holes. The 1.0Co–500TiO_2 showed better photocatalytic activity because a moderate T_{cal} is beneficial for crystallization, and the mixed anatase–rutile crystal structure of this catalyst can promote separation of photo-excited electrons and holes (Fig. 1, Table 1). At 600°C, the TiO_2 transformed into the rutile phase completely, the crystal size became larger and the S_{BET} decreased severely (Fig. 1 and Table 1). All of these are harmful for photocatalysis of RhB. Therefore, the order of photocatalytic activity is 1.0Co–500TiO_2 > 1.0–600TiO_2 > 1.0Co–400TiO_2. Having both relatively

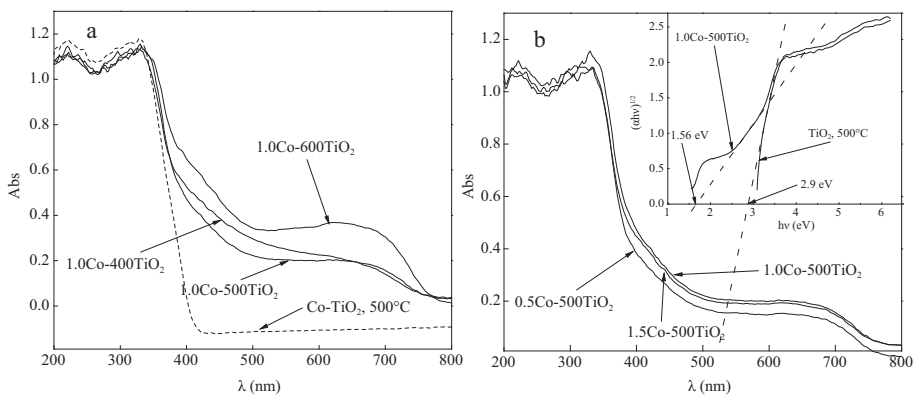

Fig. 6 – UV–vis DRS of pure TiO_2 (a) and 1.0Co–500TiO_2 (b). Insert: band gap calculated by Kubelka–Munk function.

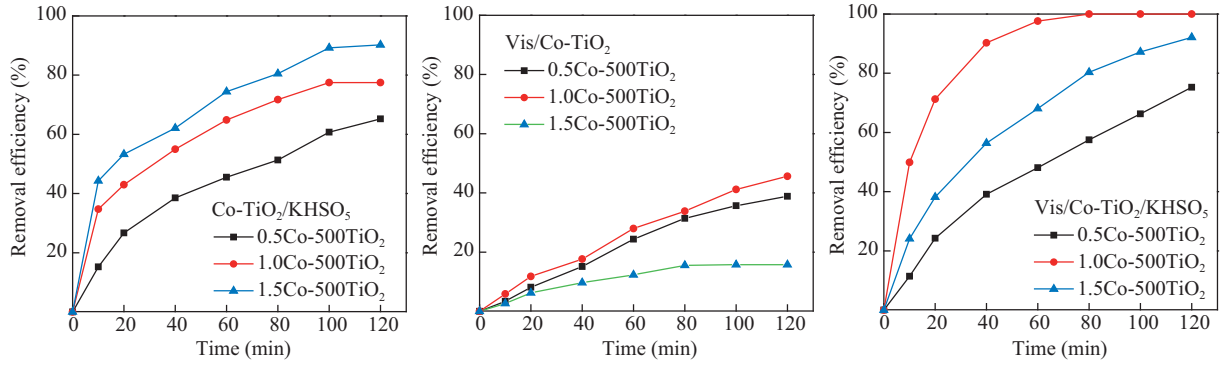

Fig. 7 – Effect of cobalt concentration (C_{cobalt}) on the degradation efficiency of RhB. Conditions: [RhB] = 50 mg/L (0.1 mmol), [$KHSO_5$] = 0.4 mmol, [Cata] = 1.0 g/L, pH = 7.0, 25°C, 2 hr.

better SR-Fenton and photocatalytic activity made 1.0–500TiO_2 perform better in the combined Fenton–Photo process. So, the optimal calcinations temperature is 500°C.

2.5. Contribution of the homogenous process

There is still controversy concerning the catalytic mechanism of some heterogeneous SR-Fenton processes. Many investigators have pointed out that the catalytic activity of heterogeneous SR-Fenton catalysts, such as Fe_3O_4 and Fe_2O_3, were partly due to leached Fe^{2+} ions. So, we have a reason to believe that the SR-Fenton activity of Co–TiO_2 may also, to some extent, originate from leached cobalt ions. To rule out the possibility that the observed catalytic activity was caused by the leaching of the prepared catalyst, the particles were removed by centrifugation to obtain a leaching solution. The concentrations of leached cobalt ions of Co–TiO_2 found by using AAS are listed in Table 3. A homogeneous process experiment was carried out using the same concentration of cobalt ions that were leached out from the catalysts. The homogeneous reaction (Co^{2+}/$KHSO_5$) contributes more when C_{cobalt} is 1.5% and T_{cal} is 400°C. When using 1.0Co–400TiO_2, the RhB removal rate of the homogeneous process was 66.7%, and the rate of the heterogeneous system was 86.6%, thus its catalytic activity may be mostly attributed to the Co^{2+} ions. However, the degradation efficiency of the homogeneous process using 1.0Co–500TiO_2 was 23.2%, which was much less than the 100% removal achieved in the heterogeneous system. Therefore, its catalytic activity was mostly ascribed to the Co–TiO_2 catalyst but not the dissolved cobalt ions. Finally, we can find that visible light did not obviously affect the RhB removal efficiency in the homogeneous Co^{2+}/$KHSO_5$ process (Fig. S3).

2.6. Catalyst reusability

The important factors for the economic viability and environmental compatibility of Co–TiO_2 are its reusability and stability. The reuse of the best sample (1.0Co–500TiO_2) was tested and shown in Fig. 9. The activity of the catalyst (RhB degradation efficiency and TOC removal) dropped slightly with repeated runs. This is mainly due to poisoning of the catalyst by reaction by-products formed in the pollutant breakdown, which are adsorbed onto the surface of the catalyst. Another reason is the agglomeration of the catalyst during the centrifugation process during recovery, as observed for other heterogeneous catalysts (Li and Zhang, 2010). So, the best sample was found to have good reusability.

2.7. Stability of Co–TiO_2

The stability includes both the structural stability of the catalyst and cobalt leaching from the catalyst. The extent of cobalt loss from fresh catalysts in the Vis/Co–TiO_2/$KHSO_5$

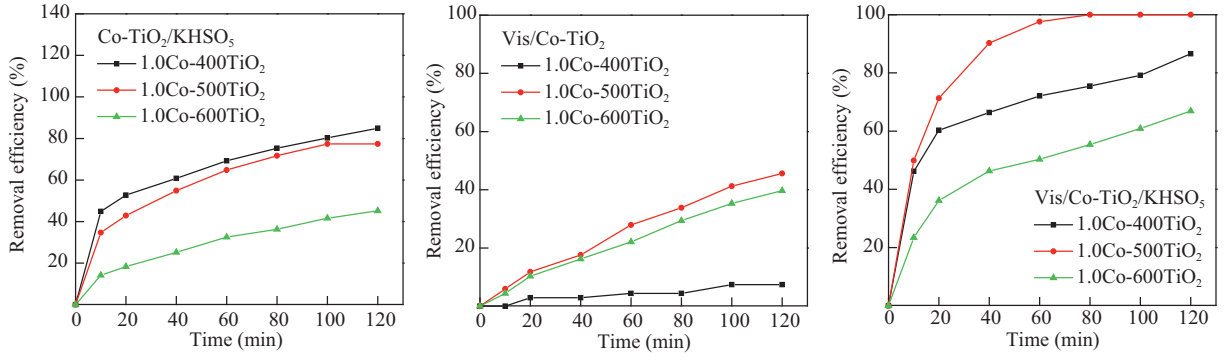

Fig. 8 – Effect of catalyst calcination temperature on the degradation efficiency of RhB. Condition: [RhB] = 50 mg/L (0.1 mmol), [$KHSO_5$] = 0.4 mmol, [Cata] = 1.0 g/L, pH = 7.0, 25°C, 2 hr.

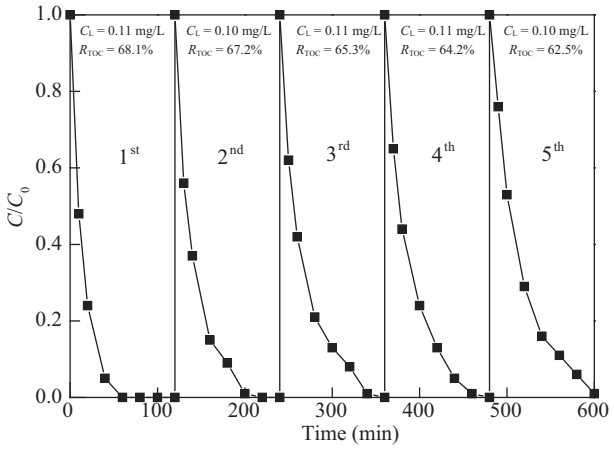

Fig. 9 – RhB degradation, TOC removal and Co^{2+} leaching in the tests of recycled Co–TiO_2 catalyst. Condition: 1.0Co–500TiO_2 used, [RhB] = 50 mg/L (0.1 mmol), [$KHSO_5$] = 0.4 mmol, [Cata] = 1.0 g/L, pH = 7.

process is listed in Table 3. In addition, Fig. S3 shows the Co^{2+} leaching of Co–TiO_2 with time. The Co^{2+} leaching of all samples stabilized after 40 min, except for 1.0Co–400TiO_2. Furthermore, the cobalt loss extent of 1.0Co–400TiO_2 among the five samples was also the most severe. This phenomenon should be due to its poor crystallinity, thus causing low mechanical strength. Thus, low T_{cal} will result in poor stability. Relatively speaking, the samples calcined at 500 and 600°C had good stability. We also monitored the Co^{2+} leaching concentration of the best sample (1.0Co–500TiO_2) in 5 runs of reuse (Fig. 9) and the structure change with XRD (Fig. S4a). It was observed that Co–TiO_2 maintains its crystalline structure, without any changes in the position and intensity of the major diffraction peaks. The concentration of the dissolved cobalt ions from Co–TiO_2 in five runs did not fluctuate notably. Finally, the lack of significant change in the surface condition of Co–TiO_2 before and after the reaction was supported by the XPS (Fig. S4b–d) analysis. So, the stability of 1.0Co–500TiO_2 is good.

2.8. Model of the catalyst and mechanism of the SR-Fenton/Vis-Photo combined system

Activation of $KHSO_5$ with cobalt usually generates two major kinds of radical, *viz.*, $^{\cdot}OH$ and $SO_4^{\cdot-}$. Fig. S5 shows the rate of RhB oxidation under the influence of the quenching reagents ethanol and tertiary butanol. Ethanol is widely used as the scavenger of $^{\cdot}OH$ and $SO_4^{\cdot-}$ while tertiary butanol is an effective quenching agent for $^{\cdot}OH$ only. In the absence of alcohol additive, about 82.7% of RhB was degraded. However, a 46.3% and a 31.4% drop in the degradation efficiency were observed in the presence of ethanol and tertiary butanol, respectively. The addition of tertiary butanol decreased the degradation efficiency of RhB significantly, indicating that $^{\cdot}OH$ was responsible for the removal of RhB. Considering that tertiary butanol is a scavenger of $^{\cdot}OH$ and its reactivity towards $SO_4^{\cdot-}$ is inefficient, the degradation of RhB in the presence of tertiary butanol could be primarily ascribed to $SO_4^{\cdot-}$. The further decrease in degradation efficiency in the presence of ethanol as $^{\cdot}OH$ and $SO_4^{\cdot-}$ scavenger confirmed the existence of $SO_4^{\cdot-}$. The results provided evidence for the involvement of both $^{\cdot}OH$ and $SO_4^{\cdot-}$ mechanisms in the Vis/Co–TiO_2/$KHSO_5$ process. The oxidation capability of this combined radical system may be more powerful than a single one.

What role did Co, TiO_2 and $KHSO_5$ play in the SR-Fenton/Vis-Photo combined system? First, from Fig. 10, a part of Co^{2+} is incorporated into the TiO_2 lattice and the remaining Co_3O_4 is immobilized on the surface of TiO_2. TiO_2 is the best support on which to load the Co_3O_4, as their interaction is relatively strong (Yang et al., 2008). The cobalt in Co_3O_4 appears in two oxidation states (Co(II) in CoO and Co(III) in Co_2O_3), and that is why Co–TiO_2 has SR-Fenton activity (Eqs. (4) and (5)).

$$Co^{2+} + HSO_5^- \rightarrow Co^{3+} + SO_4^{\cdot-} + OH^- \quad (4)$$

$$Co^{3+} + HSO_5^- \rightarrow Co^{2+} + SO_5^{\cdot-} + OH^+ \quad (5)$$

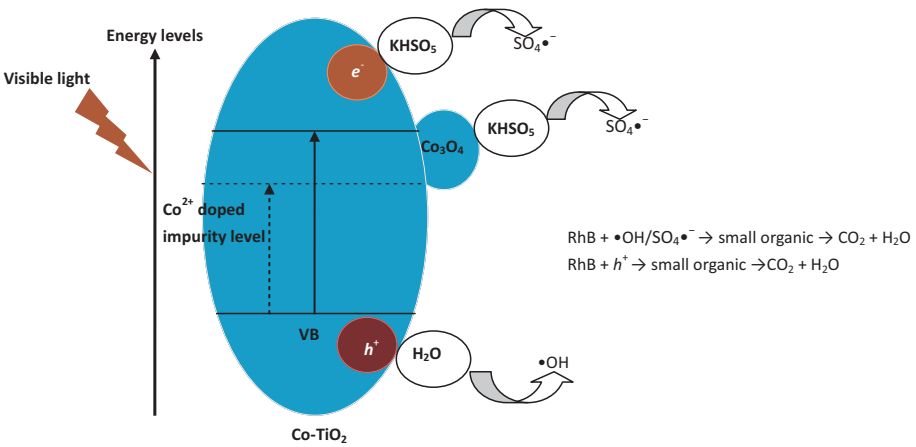

Fig. 10 – Model of Co–TiO_2 catalyst. (1) A part of Co^{2+} ions doped into TiO_2 lattice and the impurity level was formed, so the Co–TiO_2 can be excited by visible light; (2) a part of Co^{2+} ions formed Co_3O_4 on the surface of TiO_2, so Co–TiO_2 can activate $KHSO_5$ to generate $SO_4^{\cdot-}$.

Some cobalt ions are doped into the TiO_2 lattice, the 3d orbital of cobalt incorporated into TiO_2 may narrow the band gap, so that Co–TiO_2 catalysts possess visible light photocatalytic activity. In addition, the electron (hole) transfer between the cobalt ions and TiO_2 can reduce e_{cb}^-/h_{vb}^+ recombination (Eqs. (6) and (7)).

$$Co^{3+} + e_{cb}^- \rightarrow Co^{2+} \quad (6)$$

$$Co^{2+} + h_{vb}^+ \rightarrow Co^{3+} \quad (7)$$

So, the photocatalytic activity was enhanced effectively and the separation also makes VB holes more available for oxidation of adsorbed organic compounds, and for oxidation of surface hydroxyl groups and adsorbed water molecules to form ·OH (Eqs. (8) and (9)).

$$h_{vb}^+ + H_2O \rightarrow {\cdot}OH + H^+ \quad (8)$$

$$h_{vb}^+ + OH^- \rightarrow {\cdot}OH \quad (9)$$

Apart from Co and TiO_2, $KHSO_5$ also plays a significant role in the SR-Fenton/Vis-Photo combined system. As observed in Fig. S6, an interesting observation was made in regard to the change in $KHSO_5$ concentration. Visible light promoted the consumption of $KHSO_5$, suggesting that photocatalysis decomposed more $KHSO_5$. $KHSO_5$ can be used as an electron acceptor, as has been reported by some researchers, so we have a reason to believe that $KHSO_5$ also enhances the photocatalytic performance of Co–TiO_2 by inhibiting photo-excited electron–hole pair recombination, and it also means more $SO_4^{\cdot-}$ and ·OH may be generated (Eqs. (10)–(12)).

$$HSO_5^- + e_{cb}^- \rightarrow SO_4^{\cdot-} + OH^- \quad (10)$$

$$HSO_5^- + e_{cb}^- \rightarrow {\cdot}OHs + SO_4^{2-} \quad (11)$$

$$SO_4^{\cdot-} + H_2O \rightarrow SO_4^{2-} + {\cdot}OH + H^+ \quad (12)$$

Consequently, we can say that the synergistic effect observed in SR-Fenton/Vis-Photo combined system arises from the mutual promotion of heterogeneous SR-Fenton and Vis-Photo reactions.

3. Conclusions

A Co–TiO_2 catalyst was prepared using a sol–gel method. It has both SR-Fenton and visible light photocatalytic activity for the degradation of Rhodamine B at neutral pH. So, it can be defined as a type of bifunctional catalyst. In the simultaneous presence of Co–TiO_2, $KHSO_5$ and visible light, a new heterogeneous combined SR-Fenton/Vis-Photo system was formed and a synergistic effect of SR-Fenton and visible light TiO_2-photocatalysis was observed. This study may provide a useful route to develop new types of AOTs for degradation of organic pollutants.

Acknowledgments

This study was supported by the Fundamental Research Funds for the Central Universities (No. CDJXS12210002), the Major Project Foundation of Science and Technology Innovation in Minister of Education (No. 708071), the Financial Supports of the National Natural Science Foundation of China (No. 51108483), Natural Science Foundation Project of CQ CSTC (No. cstcjjA20002), and the 111 Project (No. B13041).

Appendix A. Supplementary data

Supplementary data to this article can be found online at http://dx.doi.org/10.1016/j.jes.2014.03.003.

REFERENCES

Anderson, C., Bard, A.J., 1995. An improved photocatalyst of TiO_2/SiO_2 prepared by a sol–gel synthesis. J. Phys. Chem. 99 (24), 9882–9885.

Anipsitakis, G.P., Dionysiou, D.D., 2004. Radical generation by the interaction of transition metals with common oxidants. Environ. Sci. Technol. 38 (13), 3705–3712.

Anipsitakis, G.P., Stathatos, E., Dionysiou, D.D., 2005. Heterogeneous activation of oxone using Co_3O_4. J. Phys. Chem. B 109 (27), 13052–13055.

Anipsitakis, G.P., Dionysiou, D.D., Gonzalez, M.A., 2006. Cobalt-mediated activation of peroxymonosulfate and sulfate radical attack on phenolic compounds. Implic. Chlor. Ions. Environ. Sci. Technol. 40 (3), 1000–1007.

Buxton, G.V., Greenstock, C.L., Helman, W.P., Ross, A.B., Tsang, W., 1988. Critical review of rate constants for reactions of hydrated electrons, hydrogen atoms and hydroxyl radicals (·OH/·O–) in aqueous solution. J. Phys. Chem. Ref. Data 17 (2), 513–886.

Cao, C.L., Hu, C.G., Shen, W.D., Wang, S.X., Wang, J.L., Tian, Y.S., 2013. Fabrication of a novel heterostructure of Co_3O_4-modified TiO_2 nanorod arrays and its enhanced photoelectrochemical property. J. Allergy Comp. 550, 137–143.

Chan, K.H., Chu, W., 2009. Degradation of atrazine by cobalt-mediated activation of peroxymonosulfate: different cobalt counteranions in homogenous process and cobalt oxide catalysts in photolytic heterogeneous process. Water Res. 43 (9), 2513–2521.

Ding, Y.B., Zhu, L.H., Huang, A.Z., Zhao, X.R., Zhang, X.Y., Tang, H.Q., 2012. A heterogeneous Co_3O_4–Bi_2O_3 composite catalyst for oxidative degradation of organic pollutants in the presence of peroxymonosulfate. Catal. Sci. Technol. 2 (9), 1977–1984.

Ganesh, I., Gupta, A.K., Kumar, P.P., Chandra-Sekhar, P.S., Radha, K., Padmanabham, G., et al., 2012. Preparation and characterization of Co-doped TiO_2 materials for solar light induced current and photocatalytic applications. Mater. Chem. Phys. 135 (1), 220–234.

Gao, Y.Y., Gan, H.H., Zhang, G.K., Guo, Y.D., 2013. Visible light assisted Fenton-like degradation of rhodamine B and 4-nitrophenol solutions with a stable poly-hydroxyl-iron/sepiolite catalyst. Chem. Eng. J. 217, 221–230.

Goulden, P.D., Anthony, D.H.J., 1978. Kinetics of uncatalyzed peroxydisulfate oxidation of organic matter in fresh water. Anal. Chem. 50 (7), 953–958.

Hillier, S., 2000. Accurate quantitative analysis of clay and other minerals in sandstones by XRD: comparison of a Rietveld and a reference intensity ratio (RIR) method and the importance of sample preparation. Clay Miner. 35 (1), 291–302.

Hu, X.B., Xu, X., Ji, F.Y., Fan, Z.H., 2009. Preparation and catalytic kinetic of hydrophobic photocatalytic catalysts. J. Inorg. Mater. 24 (6), 115–1120.

Huang, W., Zuo, Z.J., Han, P.D., Li, Z.H., Zhao, T.D., 2009. XPS and XRD investigation of Co/Pd/TiO_2 catalysts by different preparation methods. J. Electron. Spect. Relat. Phenom. 173 (2–3), 88–95.

Jayakumar, O.D., Sudakar, C., Persson, C., Sudarsan, V., Sakuntala, T., Naik, R., et al., 2009. 1D morphology stabilization and enhanced magnetic properties of Co:ZnO nanostructures on Codoping with Li: a template-free synthesis. Cryst. Grow. Des. 9 (10), 4450–4455.

Ji, F., Li, C.L., Deng, L., 2011. Performance of CuO/Oxone system: heterogeneous catalytic oxidation of phenol at ambient conditions. Chem. Eng. J. 178, 239–243.

Kim, Y.D., Cooper, S.L., Klein, M.V., Jonker, B.T., 1994. Spectroscopic ellipsometry study of the diluted magnetic semiconductor system Zn (Mn, Fe, Co) Se. Phys. Rev. B 49 (3), 1732–1742.

Le, T.T., Akhtar, M.S., Park, D.M., Lee, J.C., Yang, O.B., 2012. Water splitting on rhodamine-B dye sensitized Co-doped TiO_2 catalyst under visible light. Appl. Catal. B. 111–112, 397–401.

Lee, J.M., Kim, M.S., Hwang, B.H., Bae, W.K., Kim, B.W., 2003. Photodegradation of acid red 114 dissolved using a photo-Fenton process with TiO_2. Dyes Pigments 56 (1), 59–67.

Li, Y., Zhang, F.S., 2010. Catalytic oxidation of methyl orange by an amorphous FeOOH catalyst developed from a high iron-containing fly ash. Chem. Eng. J. 158 (2), 148–153.

Liang, C.J., Wang, Z.S., Bruell, C.J., 2007. Influence of pH on persulfate oxidation of TCE at ambient temperatures. Chemosphere 66 (1), 106–113.

Liu, X.H., He, X.B., Fu, Y.B., 2008. Effects of doping cobalt on the structures and performances of TiO_2 photocatalyst. Acta Chim. Sin. 66 (14), 1725–1730.

Liu, S.Q., Feng, L.R., Xu, N., Chen, Z.G., Wang, X.M., 2012. Magnetic nickel ferrite as a heterogeneous photo-Fenton catalyst for the degradation of rhodamine B in the presence of oxalic acid. Chem. Eng. J. 203, 432–439.

Long, M.C., Cai, W.M., Cai, J., Zhou, B.X., Chai, X.Y., Wu, Y.H., 2006. Efficient photocatalytic degradation of phenol over Co_3O_4/$BiVO_4$ composite under visible light irradiation. J. Phys. Chem. B 110 (41), 20211–20216.

Lu, Y.C., Lin, Y.H., Wang, D.J., Wang, L.L., Xie, T.F., Jiang, T.F., 2011. A high performance cobalt-doped ZnO visible light photocatalyst and its photogenerated charge transfer properties. Nano Res. 4 (11), 1144–1152.

Ma, Y., Yao, J.N., 1999. Comparison of photodegradative rate of rhodamine B assisted by two kinds of TiO_2 films. Chemosphere 38 (10), 2407–2414.

Muhammad, S., Saputra, E., Sun, H.Q., Izidoro, J.C., Fungaro, D.A., Ang, H.M., et al., 2012. Coal fly ash supported Co_3O_4 catalysts for phenol degradation using peroxymonosulfate. RSC Adv. 2 (13), 5645–5650.

Quici, N., Morgada, M.E., Piperata, G., Babay, P., Gettar, R.P., Litter, M.I., 2005. Oxalic acid destruction at high concentrations by combined heterogeneous photo-catalysis and photo-Fenton processes. Catal. Today 101 (3–4), 253–260.

Ram, M.K., Andreescu, S., Ding, H.M., 2011. Nanotechnology for Environmental Decontamination. McGraw-Hill Professional, New York, pp. 173–175.

Rey, A., Carbajo, J., Adán, C., Faraldos, M., Bahamonde, A., Casas, J.A., et al., 2011. Improved mineralization by combined advanced oxidation processes. Chem. Eng. J. 174 (1), 134–142.

Selvam, K., Muruganandham, M., Sobana, N., Swaminathan, M., 2007. Enhancement of UV-assisted photo-Fenton degradation of reactive orange 4 using TiO_2–P25 nanoparticles. Sep. Purif. Technol. 54 (2), 241–247.

Shen, X.T., Zhu, L.H., Li, J., Tang, H.Q., 2007. Synthesis of molecular imprinted polymer coated photocatalysts with high selectivity. Chem. Commun. 11, 1163–1165.

Shen, X.T., Zhu, L.H., Huang, C.X., Tang, H.Q., Yu, Z.W., Deng, F., 2009. Inorganic molecular imprinted titanium dioxide photocatalyst: synthesis, characterization and its application for efficient and selective degradation of phthalate esters. J. Mater. Chem. 19 (27), 4843–4851.

Shi, P.H., Su, R.J., Wan, F.Z., Zhu, M.C., Li, D.X., Xu, S.H., 2012. Co_3O_4 nanocrystals on graphene oxide as a synergistic catalyst for degradation of orange II in water by advanced oxidation technology based on sulfate radicals. Appl. Catal. B. 123–124, 265–272.

Shukla, P., Wang, S.B., Singh, K., Ang, H.M., Tadé, M.O., 2010. Cobalt exchanged zeolites for heterogeneous catalytic oxidation of phenol in the presence of peroxymonosulphate. Appl. Catal. B. 99 (1–2), 163–169.

Sridharan, K., Park, T.J., 2013. Thorn-ball shaped TiO_2 nanostructures: influence of Sn^{2+} doping on the morphology and enhanced visible light photocatalytic activity. Appl. Catal. B. 134–135, 174–184.

Wang, F., Zhang, K., 2011. Reduced graphene oxide-TiO_2 nanocomposite with high photocatalystic activity for the degradation of rhodamine B. J. Mol. Catal. A. 345 (1), 101–107.

Xu, Z., 2010. Photocatalytic-biochemical Wastewater Treatment Based on the Characterization of Refractory Organic Pollutants(PhD thesis.) Chongqing University, pp. 31–33.

Yang, Q.J., Choi, H., Dionysiou, D.D., 2007. Nanocrystalline cobalt oxide immobilized on titanium dioxide nanoparticles for the heterogeneous activation of peroxymonosulfate. Appl. Catal. B. 74 (1–2), 170–178.

Yang, Q.J., Choi, H., Chen, Y.J., Dionysiou, D.D., 2008. Heterogeneous activation of peroxymonosulfate by supported cobalt catalysts for the degradation of 2,4-dichlorophenol in water: the effect of support, cobalt precursor, and UV radiation. Appl. Catal. B. 77 (3–4), 300–307.

Zayat, M., Levy, D., 2000. Blue $CoAl_2O_4$ particles prepared by the Sol–gel and citrate–gel methods. Chem. Mater. 12 (9), 2763–2769.

Editorial Board of Journal of Environmental Sciences

JOURNAL OF ENVIRONMENTAL SCIENCES

环境科学学报(英文版)

(http://www.jesc.ac.cn)

Aims and scope

Journal of Environmental Sciences is an international academic journal supervised by Research Center for Eco-Environmental Sciences, Chinese Academy of Sciences. The journal publishes original, peer-reviewed innovative research and valuable findings in environmental sciences. The types of articles published are research article, critical review, rapid communications, and special issues.

The scope of the journal embraces the treatment processes for natural groundwater, municipal, agricultural and industrial water and wastewaters; physical and chemical methods for limitation of pollutants emission into the atmospheric environment; chemical and biological and phytoremediation of contaminated soil; fate and transport of pollutants in environments; toxicological effects of terrorist chemical release on the natural environment and human health; development of environmental catalysts and materials.

For subscription to electronic edition

Elsevier is responsible for subscription of the journal. Please subscribe to the journal via http://www.elsevier.com/locate/jes.

For subscription to print edition

China: Please contact the customer service, Science Press, 16 Donghuangchenggen North Street, Beijing 100717, China. Tel: +86-10-64017032; E-mail: journal@mail.sciencep.com, or the local post office throughout China (domestic postcode: 2-580).

Outside China: Please order the journal from the Elsevier Customer Service Department at the Regional Sales Office nearest you.

Submission declaration

Submission of an article implies that the work described has not been published previously (except in the form of an abstract or as part of a published lecture or academic thesis), that it is not under consideration for publication elsewhere. The submission should be approved by all authors and tacitly or explicitly by the responsible authorities where the work was carried out. If the manuscript accepted, it will not be published elsewhere in the same form, in English or in any other language, including electronically without the written consent of the copyright-holder.

Submission declaration

Submission of the work described has not been published previously (except in the form of an abstract or as part of a published lecture or academic thesis), that it is not under consideration for publication elsewhere. The publication should be approved by all authors and tacitly or explicitly by the responsible authorities where the work was carried out. If the manuscript accepted, it will not be published elsewhere in the same form, in English or in any other language, including electronically without the written consent of the copyright-holder.

Editorial

Authors should submit manuscript online at http://www.jesc.ac.cn. In case of queries, please contact editorial office, Tel: +86-10-62920553, E-mail: jesc@263.net, jesc@rcees.ac.cn. Instruction to authors is available at http://www.jesc.ac.cn.

Journal of Environmental Sciences (Established in 1989)

Vol. 26 No. 12 2014

Supervised by	Chinese Academy of Sciences	**Published by**	Science Press, Beijing, China
Sponsored by	Research Center for Eco-Environmental		Elsevier Limited, The Netherlands
	Sciences, Chinese Academy of Sciences	**Distributed by**	
Edited by	Editorial Office of Journal of	Domestic	Science Press, 16 Donghuangchenggen
	Environmental Sciences		North Street, Beijing 100717, China
	P. O. Box 2871, Beijing 100085, China		Local Post Offices through China
	Tel: 86-10-62920553; http://www.jesc.ac.cn	Foreign	Elsevier Limited
	E-mail: jesc@263.net, jesc@rcees.ac.cn		http://www.elsevier.com/locate/jes
Editor-in-chief	Hongxiao Tang	**Printed by**	Beijing Beilin Printing House, 100083, China

CN 11-2629/X **Domestic postcode: 2-580** **Domestic price per issue RMB ¥ 110.00**

ISSN 1001-0742